

KamLAND, neutrino transition magnetic moments and the solar magnetic field

V. Antonelli^{a*}, Bhag C. Chauhan^{b*1}, João Pulido^{b*}, E. Torrente-Lujan^{c*}

^a *Dip. di Fisica, Univ. di Milano, and INFN Sez. Milano, Via Celoria 16, Milano, Italy*

^b *Centro de Física das Interações Fundamentais (CFIF), Departamento de Física, Instituto Superior Técnico, Av. Rovisco Pais, P-1049-001 Lisboa, Portugal*

^c *Departamento de Física, Grupo de Física Teórica, Universidad de Murcia, Murcia, Spain.*

Abstract

We present here a recopilation of recent results about the possibility of detecting solar electron antineutrinos produced by solar core and convective magnetic fields. These antineutrinos are predicted by spin-flavor oscillations at a significant rate even if this mechanism is not the leading solution to the SNP. Using the recent Kamland results and assuming a concrete model for antineutrino production by spin-flavor precession in the convective zone based on chaotic magnetic fields, we obtain bounds on the flux of solar antineutrinos, on the average conversion neutrino-antineutrino probability and on intrinsic neutrino magnetic moment. In the most conservative case, $\mu \leq 2.5 \times 10^{-11} \mu_B$ (95% CL). When studying the effects of a core magnetic field, we find in the weak limit a scaling of the antineutrino probability with respect to the magnetic field profile in the sense that the same probability function can be reproduced by any profile with a suitable peak field value. In this way the solar electron antineutrino spectrum can be unambiguously predicted. We use this scaling and the negative results indicated by the KamLAND experiment to obtain upper bounds on the solar electron antineutrino flux. We find that, for a wide family of magnetic field profiles in the sun interior, the antineutrino appearance probability is largely determined by the magnetic field intensity but not by its shape. Explicit limits on neutrino transition moments are also obtained consistent with the convective case. These limits are therefor largely independent of the detailed structure of the magnetic field in the solar interior.

Expanded version of the presentation contributed to “ 8th International Workshop On Topics In Astroparticle And Underground Physics (TAUP 2003)”

¹On leave from Govt. Degree College, Karsog (H P) India 171304.

1 Introduction

Evidence of electron antineutrino disappearance in a beam of antineutrinos in the KamLAND experiment has been recently presented [1]. The analysis of these results [1, 2] in terms of neutrino oscillations have largely improved our knowledge of neutrino mixing in the LMA region. The results appear to confirm in an independent way that the observed deficit of solar neutrinos is indeed due to neutrino oscillations. The ability to measure the LMA solution, the one preferred by the solar neutrino data at present, “in the lab” puts KamLAND in a pioneering situation: after these results there should remain little doubt of the physical reality of neutrino mass and oscillations. Once neutrino mass is observed, neutrino magnetic moments are an inevitable consequence in the Standard Model and beyond. Magnetic moment interactions arise in any renormalizable gauge theory only as finite radiative corrections: the diagrams which contribute to the neutrino mass will inevitably generate a magnetic moment once the external photon line is added.

The spin flavor precession (SFP) [3–5], based on the interaction of the neutrino magnetic moment with the solar magnetic field was, second to oscillations, the most attractive scenario [19]. SFP, although certainly not playing the major role in the solar neutrino deficit, may still be present as a subdominant process, provided neutrinos have a sizeable transition magnetic moment. Its signature will be the appearance of solar antineutrinos [4, 6, 18] which result from the combined effect of the vacuum mixing angle θ and the transition magnetic moment μ_ν converting neutrinos into antineutrinos of a different flavor. This can be schematically shown as

$$\nu_{eL} \rightarrow \nu_{\mu L} \rightarrow \bar{\nu}_{eR}, \quad (1)$$

$$\nu_{eL} \rightarrow \bar{\nu}_{\mu R} \rightarrow \bar{\nu}_{eR} \quad (2)$$

with oscillations acting first and SFP second in sequence (1) and in reverse order in sequence (2). Oscillations and SFP can either take place in the same spatial region, or be spatially separated. Independently of their origin, antineutrinos with energies above 1.8 MeV can be detected in KamLAND via the observation of positrons from the inverse β -decay reaction $\bar{\nu}_e + p \rightarrow n + e^+$ and must all be originated from 8B neutrinos.

The KamLAND experiment is the successor of previous reactor experiments (CHOOZ [8], PaloVerde [9]) at a much larger scale in terms of baseline distance and total incident flux. This experiment relies upon a 1 kton liquid scintillator detector located at the old, enlarged, Kamiokande site. It searches for the oscillation of antineutrinos emitted by several nuclear power plants in Japan. The nearby 16 (of a total of 51) nuclear power stations deliver a $\bar{\nu}_e$ flux of $1.3 \times 10^6 \text{ cm}^{-2} \text{ s}^{-1}$ for neutrino energies $E_\nu > 1.8$ MeV at the detector position. About 85% of this flux comes from reactors forming a well defined baseline of 139–344 km. Thus, the flight range is limited in spite

of using several reactors, because of this fact the sensitivity of KamLAND increases by nearly two orders of magnitude compared to previous reactor experiments.

Beyond reactor neutrino measurements, the secondary physics program of KamLAND includes diverse objectives as the measurement of geoneutrino flux emitted by the radioactivity of the earth's crust and mantle, the detection of antineutrino bursts from galactic supernova and, after extensive improvement of the detection sensitivity, the detection of low energy ${}^7\text{Be}$ neutrinos using neutrino-electron elastic scattering.

Moreover, the KamLAND experiment is capable of detecting potential electron antineutrinos produced on fly from solar ${}^8\text{B}$ neutrinos [18]. These antineutrinos are predicted by spin-flavor oscillations at a significant rate if the neutrino is a Majorana particle and if its magnetic moment is high enough [19, 20]. In Ref.[18] as been remarked that the flux of reactor antineutrinos at the Kamiokande site is comparable, and in fact smaller, to the flux of ${}^8\text{B}$ neutrinos emitted by the sun $\Phi({}^8\text{B}) \simeq 5.6 \times 10^6 \text{ cm}^{-2} \text{ s}^{-1}$ [1, 21, 22]. Their energy spectrum is important at energies $2 - 4$ MeV while solar neutrino spectrum peaks at around $9 - 10$ MeV. As the inverse beta decay reaction cross section increases as the square of the energy, we would expect nearly 10 times more solar electron antineutrino events even if the initial fluxes were equal in magnitude.

The publication of the SNO results [22, 23] has already made an important breakthrough towards the solution of the long standing solar neutrino [28, 29, 33, 34] problem (SNP) possible. These results provide the strongest evidence so far (at least until KamLAND improves its statistics) for flavor oscillation in the neutral lepton sector.

The existing bounds on solar electron antineutrinos are strict. The present upper limit on the absolute flux of solar antineutrinos originated from ${}^8\text{B}$ neutrinos is [18, 36, 37] $\Phi_{\bar{\nu}}({}^8\text{B}) < 1.8 \times 10^5 \text{ cm}^{-2} \text{ s}^{-1}$ which is equivalent to an averaged conversion probability bound of $P < 3.5\%$ (SSM-BP98 model). There are also bounds on their differential energy spectrum [36]: the conversion probability is smaller than 8% for all $E_{e,vis} > 6.5$ MeV going down the 5% level above $E_{e,vis} \simeq 10$ MeV.

The main aim of this work is to study the implications of the recent KamLAND results on the determination of the solar electron antineutrino appearance probability, independently from concrete models on antineutrino production. We obtain upper limits on the solar antineutrino flux, the intrinsic magnetic moment and the magnetic field at the bottom of the convective zone were [18] from the published KamLAND data. In the second part of the work, we address however a different antineutrino production model where the magnetic field at the solar core is the relevant one. The purpose of this part is to relate the solar magnetic field profile to the solar antineutrino event rate in KamLAND which is a component of the total positron event rate in the reaction above. In a previous paper [7] the question of what can be learned about the strength and coordinate dependence of the solar magnetic field in relation to the current upper limits on the solar $\bar{\nu}_e$ flux was addressed. The system of equations describing neutrino evolution in the sun was solved analytically in perturbation theory for small $\mu_\nu B$,

the product of the neutrino magnetic moment by the solar field. The three oscillation scenarios with the best fits were considered, namely LMA, LOW and vacuum solutions. In particular for LMA it was found that the antineutrino probability depends only on the magnitude of the magnetic field in the neutrino production zone. Neutrinos were, in the approximation used, considered to be all produced at the same point ($x = 0.05R_S$), where 8B neutrino production is peaked. In this work we will consider the more realistic case of a convolution of the production distribution spectrum with the field profile in that region. It will be seen that this convolution leads to an insensitiveness of the antineutrino probability with respect to the solar magnetic field profile, in the sense that different profiles can correspond to the same probability function, provided the peak field values are conveniently scaled. As a consequence, an upper bound on the solar antineutrino flux can be derived which is independent of the field profile and the energy spectrum of this flux will also be seen to be profile independent.

The structure of this work is the following. In section 2 we discuss the main features of KamLAND experiment that are relevant for our analysis: The salient aspects of the procedure we are adopting and the results of our analysis are presented and discussed in sections 3. In Section 4 we apply the results we obtained in a particular model for the solar magnetic field, we obtain bounds on the values of the intrinsic neutrino transition magnetic moments. Finally, in section 5 we draw our conclusions and discuss possible future scenarios.

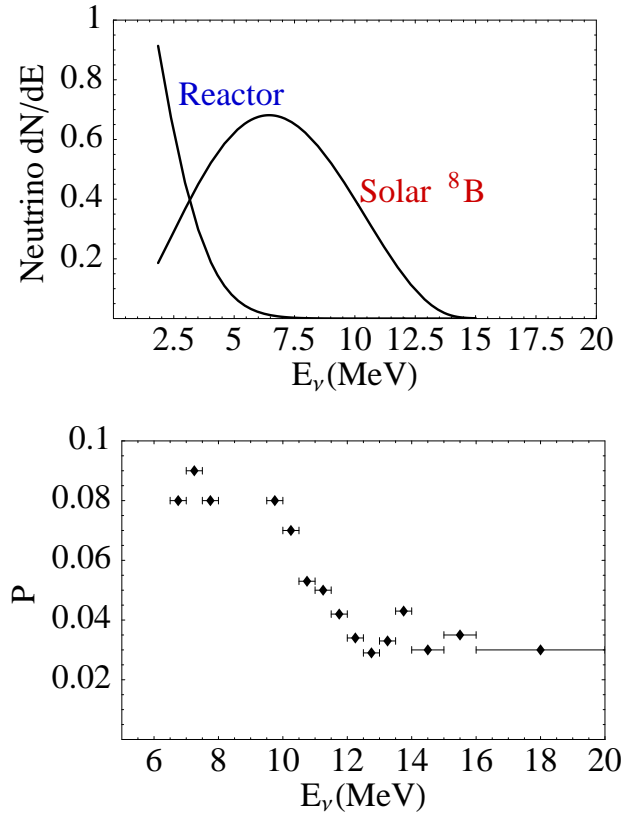


Figure 1: (Top) The reactor antineutrino and solar 8B neutrino [21] fluxes. (Bottom). Upper limits on solar antineutrino conversion probabilities (from Ref.[36]).

2 A KamLAND overview

Independently of their origin, solar or reactor electron antineutrinos from nuclear reactors with energies above 1.8 MeV can be detected in KamLAND by the inverse β -decay reaction $\bar{\nu}_e + p \rightarrow n + e^+$. The time coincidence, the space correlation and the energy balance between the positron signal and the 2.2 MeV γ -ray produced by the capture of a already-thermalized neutron on a free proton make it possible to identify this reaction unambiguously, even in the presence of a rather large background.

The main ingredients in the calculation of the corresponding expected signals in KamLAND are solar fluxes mentioned above, the reactor flux and the antineutrino cross section on protons. These last two are considered below (see also Ref.[24]).

2.1 The reactor antineutrino flux

We first describe the flux of antineutrinos coming from the power reactors. A number of short baseline experiments (Ref.[40] and references therein) have measured the energy spectrum of reactors at distances where oscillatory effects have been shown to be inexistent. They have shown that the theoretical neutrino flux predictions are reliable within 2% [42].

The effective flux of antineutrinos released by the nuclear plants is a rather well understood function of the thermal power of the reactor and the amount of thermal power emitted during the fission of a given nucleus, which gives the total amount, and the isotopic composition of the reactor fuel which gives the spectral shape. Detailed tables for these magnitudes can be found in Ref. [40].

For a given isotope (j) the energy spectrum can be parametrized by the following expression $dN_\nu^j/dE_\nu = \exp(a_0 + a_1 E_\nu + a_2 E_\nu^2)$ where the coefficients a_i depend on the nature of the fissionable isotope (see Ref.[40] for explicit values). Along the year, between periods of refueling, the total effective flux changes with time as the fuel is expended and the isotope relative composition varies. The overall spectrum is at a given time $dN_\nu/dE_\nu = \sum_{j=\text{isotopes}} c_j(t) dN_\nu^j/dE_\nu$. To compute a fuel-cycle averaged spectrum we have made use of the typical time evolution of the relative abundances c_j , which can be seen in Fig. 2 of Ref.[40]. This averaged spectrum can be again fitted very well by the same functional expression as above. The isotopic energy yield is properly taken into account. As the result of this fit, we obtain the following values which are the ones to be used in the rest of this work: $a_0 = 0.916$, $a_1 = -0.202$, $a_2 = -0.088$. Although individual variations of the c_j along the fuel cycle can be very high, the variation of the two most important ones is highly correlated: the coefficient $c(^{235}\text{U})$ increases in the range $\sim 0.5 - 0.7$ while $c(^{239}\text{Pu})$ decreases $\sim 0.4 - 0.2$. This correlation makes the effective description of the total spectrum by a single expression as above useful. With the fitted coefficients a_i above, the difference between this effective spectrum and the

real one is typically 2 – 4% along the yearly fuel cycle.

2.2 Antineutrino cross sections

We now consider the cross sections for antineutrinos on protons. We will sketch the form of the well known differential expression and more importantly we will give updated numerical values for the transition matrix elements which appear as coefficients.

In the limit of infinite nucleon mass, the cross section for the reaction $\bar{\nu}_e + p \rightarrow n + e^+$ is given by [11, 12] $\sigma(E_{\bar{\nu}}) = k E_{e^+} p_{e^+}$ where E, p are the positron energy and momentum and k a transition matrix element which will be considered below. The positron spectrum is monoenergetic: $E_{\bar{\nu}}$ and E_{e^+} are related by: $E_{\bar{\nu}}^{(0)} = E_{e^+}^{(0)} + \Delta M$, where M_n, M_p are the neutron and proton masses and $\Delta M = M_n - M_p \simeq 1.293$ MeV.

Nucleon recoil corrections are potentially important in relating the positron and antineutrino energies in order to evaluate the antineutrino flux. Because the antineutrino flux $\Phi(E_{\nu})$ would typically decrease quite rapidly with energy, the lack of adequate corrections will systematically overestimate the positron yield. For both cases, solar or reactor antineutrinos, because the antineutrino flux $\Phi(E_{\nu})$ would typically decrease quite rapidly with energy, the lack of adequate corrections will systematically overestimate the positron yield. For the solar case and taking into account the SSM-BP98 8B spectrum, the effect decrease the positron yield by 2-8% at the main visible energy range $\sim 6 - 10$ MeV. The positron yield could decrease up 50% at *hep* neutrino energies, a region where incertitudes in the total and differential spectrum are of comparable size or larger. Finite energy resolution smearing will however diminish this correction when integrating over large enough energy bins: in the range 6.5 – 20 MeV the net positron suppression is estimated to be at the 5% level, increasing up 20% at *hep* energies.

At highest orders, the positron spectrum is not monoenergetic and one has to integrate over the positron angular distribution to obtain the positron yield. We have used the complete expressions which can be found in Ref. [10]. Here we only want to stress the numerical value of the overall coefficient σ_0 (notation of Ref.[10]) which is related to the transition matrix element k above. The matrix transition element can be written in terms of measurable quantities as $k = 2\pi^2 \log 2 / (m_e^5 f t_{1/2})$. Where the value of the space factor $f = 1.71465 \pm 0.00015$ follows from calculation [13], while $t_{1/2} = 613.9 \pm 0.55$ sec is the latest published value for the free neutron half-life [37]. This value has a significantly smaller error than previously quoted measurements. From the values above, we obtain the extremely precise value: $k = (9.5305 \pm 0.0085) \times 10^{-44} \text{ cm}^2/\text{MeV}^2$. From here the coefficient which appears in the differential cross section is obtained as (vector and axial vector couplings $f = 1, g = 1.26$): $k = \sigma_0(f^2 + 3g^2)$. In summary, the differential cross section which appear in KamLAND are very well known, its theoretical errors are negligible if updated values are employed.

3 The solar signal and reactor backgrounds

Electron antineutrinos from any source, nuclear reactors or solar origin, with energies above 1.8 MeV are measured in KamLAND by detecting the inverse β -decay reaction $\bar{\nu}_e + p \rightarrow n + e^+$. The time coincidence, the space correlation and the energy balance between the positron signal and the 2.2 MeV γ -ray produced by the capture of a already-thermalized neutron on a free proton make it possible to identify this reaction unambiguously, even in the presence of a rather large background.

The two principal ingredients in the calculation of the expected signal in KamLAND are the corresponding flux and the electron antineutrino cross section on protons. The average number of positrons N_i originated from the solar source which are detected per visible energy bin ΔE_i is given by the convolution of different quantities:

$$N_i = Q_0 \int_{\Delta E_i} dE_e \int_0^\infty dE_e^r \epsilon(E_e) R(E_e, E_e^r) \int_{E_e^r}^\infty dE_{\bar{\nu}} \bar{p}(E_{\bar{\nu}}) \Phi(E_{\bar{\nu}}) \sigma(E_{\bar{\nu}}, E_e^r) \quad (3)$$

where Q_0 is a normalization constant accounting for the fiducial volume and live time of the experiment, \bar{p} . Expressions for the electron antineutrino capture cross section $\sigma(E_{\bar{\nu}}, E_e^r)$ are taken from the literature [10, 38]. The matrix element for this cross section can be written in terms of the neutron half-life, we have used the latest published value $t_{1/2} = 613.9 \pm 0.55$ [37]. The functions $\epsilon(E_e)$ and $R(E_e, E_e^r)$ are the detection efficiency and the energy resolution function. We use in our analysis the following expression for the energy resolution in the prompt positron detection $\sigma(E_e) = 0.0062 + 0.065\sqrt{E_e}$. This expression is obtained from the raw calibration data presented in Ref.[39]. Note that we prefer to use this expression instead of the much less accurate one given in Ref.[1]. Moreover, we assume a 408 ton fiducial mass and the detection efficiency is taken independent of the energy [1], $\epsilon = 80\%$. In order to obtain concrete limits, a model should be taken which predict \bar{p} and its dependence with the energy. For our purpose it will suffice to suppose \bar{p} a constant. This is justified at least in two cases: a) if the energy range ΔE over which we perform the integration is small enough so the variation of the probability is not very large, or b) if we reinterpret \bar{p} as an energy-averaged probability, note that, in a general case, this is always true because the un-avoidable convolution with a finite energy resolution. (see Expression 10 in Ref.[20]):

$$\bar{p}_{\Delta E} = \frac{\int_{\Delta E} dE \sigma(E) \Phi(E) P_{\bar{\nu}}(E)}{\int_{\Delta E} dE \sigma(E) \Phi(E)}. \quad (4)$$

Let us finally note that independently of the reasons above, upper limits to be obtained on continuation are still valid even if the antineutrino probabilities are significantly different from constant: if we take $\bar{p} = \max_{\Delta E} P_{\bar{\nu}}(E)$ the expected antineutrino signal computed with \bar{p} will be always larger than the signal obtained inserting the full probability.

Similarly, the expected numbers of positron events originated from power reactor neutrinos are obtained summing the expectations for all the relevant reactor sources weighting each source by its power and distance to the detector (table II in Ref. [40]), assuming the same spectrum originated from each reactor. We have used the antineutrino flux spectrum given by the expression of the previous section and the relative reactor-reactor power normalization.

For one year of running with the 600 ton fiducial mass and for standard nuclear plant power and fuel schedule: we assume all the reactors operated at $\sim 80\%$ of their maximum capacity and an averaged, time-independent, fuel composition equal for each detector, the experiment expects about 550 antineutrino events.

In addition to the reactor antineutrino signal deposited in the detector, two classes of other backgrounds can be distinguished [14, 40, 42]. The so called random coincidence background is due to the contamination of the detector scintillator by U, Th and Rn. From MC studies and assuming that an adequate level of purification can be obtained, the background coming from this source is expected to be ~ 0.15 events/d/kt which is equivalent to a signal to background ratio of $\sim 1\%$. Other works [26] conservatively estimate a 5% level for this ratio. More importantly for what it follows, one expects that the random coincidence backgrounds will be a relatively steeply falling function of energy. The assumption of no random coincidence background should be relatively safe at high energies above ~ 5 MeV which are those of interest here.

The second source of background, the so called correlated background is dominantly caused by cosmic ray muons and neutrons. The KamLAND's depth is the main tool to suppress those backgrounds. MC methods estimate a correlated background of around 0.05 events/day/kt distributed over all the energy range up to ~ 20 MeV, this is the quantity that we will consider later.

In order to estimate the sensitivity of KamLAND to put limits on the flux of antineutrinos arriving from the sun we have computed the expected signals coming from solar and reactor antineutrinos and from the background. They are presented in Table (1) for different representative values of the minimum energy required (E_{thr}) for the visible positrons. We have supposed a background of 0.05 evt/d/kt uniformly distributed over the full energy range. To obtain the solar numbers (first column, S_{sun}) we have supposed full neutrino-antineutrino conversion ($\bar{P} = 1$) with no spectral distortion. For any other conversion probability, the experiment should see the antineutrino quantity $\bar{P} \times S_{sun}$ in addition to the reactor ones and other background. If the experiment does not receive any solar antineutrinos, making a simple statistical estimation (only statistical errors are included) we obtain the upper limits on the conversion probability which appear in the last column of the table.

From the table we see that after three years of data taking the optimal result is obtained imposing a energy detection threshold at ~ 7 MeV. A negative result would allow to impose an upper limit on the average antineutrino appearance probability at

$\sim 0.20\%$ (95% CL). The corresponding limits after one year of data taking are only slightly worse, they are respectively: 0.21-0.24% (95% CL).

The results of our simulation are summarized in Fig.3 where we show the “solar” positron spectrum obtained assuming the shape of the 8B neutrino flux and a total normalization $10^{-2} \times \Phi({}^8B)$ which means an overall $\nu_e - \bar{\nu}_e$ conversion probability $\bar{P} \sim 1\%$.

These results are obtained under the supposition of no disappearance on the reactor flux arriving to KamLAND. No flux suppression is expected for values of the mixing parameters in the LOW region, more precisely for any $\Delta m^2 \leq 2 \times 10^{-5} \text{ eV}^2$ (see Plot 1(right) in Ref.[28] and Ref.[24]). The consideration of reactor antineutrino oscillations does not change significantly the sensitivity in obtaining upper limits on \bar{P} . For values of the mixing parameters fully on the LMA region, $\Delta m^2 \geq 1 - 9 \times 10^{-5} \text{ eV}^2$, the flux suppression is typically $S/S_0 \sim 0.5 - 0.9$ and always over $S/S_0 \sim 0.4$, for any the energy threshold $E_{thr} \sim 5-8 \text{ MeV}$. We have obtained the expected reactor antineutrino contribution for a variety of points in the LMA region (see table I in Ref.[24]) and corresponding upper limits on \bar{P} : the results after 3 years of running are practically the same while for 1 year of data running are slightly better (for example \bar{P} goes down from 0.27 to 0.3 for $E_{thr} > 6 \text{ MeV}$).

E_{thr}	S_{Sun}	S_{Rct}	Bckg.	P (CL 95)%	P (CL 99)%
6 MeV	616	43	70	0.22	0.23
7 MeV	500	11	65	0.19	0.20
8 MeV	366	2	60	0.21	0.23

Table 1: Expected signals from solar antineutrinos after 3 years of data taking. Reactor antineutrino (no oscillation is assumed) and other background (correlated background) over the same period. The random coincidence background is supposed negligible above these energy thresholds. Upper limits on the antineutrino oscillation probability.

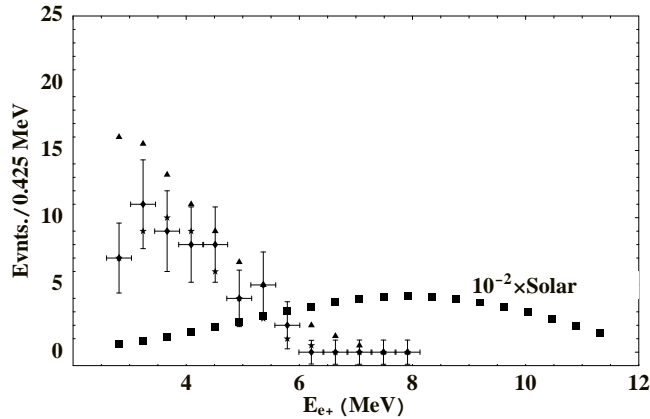


Figure 2: The KamLAND positron spectrum from reactor antineutrinos (from Fig.5 in Ref.[1]): measured (145.5 days), MC expectations in absence of oscillations and best fit including neutrino oscillations ($\Delta m^2 = 6.9 \times 10^{-5} \text{ eV}^2$, $\sin^2 \theta = 1$, respectively points with error-bars, triangles and stars). The “solar” positron spectrum (black solid squares) obtained assuming the shape of the 8B neutrino flux and a total normalization $10^{-2} \times \Phi({}^8B)$ (that is, an overall $\nu_e - \bar{\nu}_e$ conversion probability $\overline{P} \sim 1\%$).

4 Analysis and Results

We will obtain upper bounds on the solar electron antineutrino appearance probability analyzing the observed KamLAND rates in three different ways (see Refs.[15, 18], see also Refs.[16]). In the first one, we will make a standard χ^2 analysis of the observed and expected solar signals in the 13 prompt positron energy bins considered by KamLAND [1]. In the second and third cases we will apply Gaussian and poissonian probabilistic considerations to the global rate seen by the experiment and to the individual event content in the highest energy bins ($E_e > 6$ MeV) where KamLAND observes zero events. This null signal makes particularly simple the extraction of statistical conclusions in this case.

Analysis of the KamLAND Energy Spectrum

Here we fully use the binned KamLAND signal (see Fig. 5 in Ref.[1]) for estimating the parameters of solar electron antineutrino production from the method of maximum-likelihood. We minimize the quantity $\chi^2 = \chi_{i=1,9}^2 + \chi_{i=10,13}^2$ where the first term correspond to the contribution of the first nine bins where the signal is large enough and the use of the Gaussian approximation is justified. The second term correspond to the latest bins where the observed and expected signals are very small and poissonian statistics is needed. The explicit expressions are:

$$\chi_{i=1,9}^2 = \sum_{i=1,9} \frac{(S_i^{exp} - S_i^{teo})^2}{\sigma^2} \quad (5)$$

$$\chi_{i=10,13}^2 = 2 \sum_{i=10,13} S_i^{teo} - S_i^{exp} + S_i^{exp} \log \frac{S_i^{exp}}{S_i^{teo}}. \quad (6)$$

The quantities S_i are the observed bin contents from KamLAND. The theoretical signals are in principle a function of three different parameters: the solar electron antineutrino appearance probability \bar{p} and the neutrino oscillation parameters $(\Delta m^2, \theta)$. Both contributions, the contribution from solar antineutrinos and that one from solar reactors, can be treated as different summands:

$$S_i(\bar{p}, \Delta m^2, \theta) = S_i^{solar}(\bar{p}) + S_i^{reactor}(\Delta m^2, \theta). \quad (7)$$

According to our model, the solar antineutrino appearance probability \bar{p} is taken as a constant and we can finally write:

$$S_i(\bar{p}, \Delta m^2, \theta) = \bar{p} \times S_i^0 + S_i^{reactor}(\Delta m^2, \theta). \quad (8)$$

In this work we will take for the minimization values of the oscillation parameters those obtained when ignoring any solar antineutrinos (LMA solution $\Delta m^2 = 6.9 \times 10^{-5}$ eV², $\sin^2 \theta = 1$ from Ref.[1]) and we will perform a one-parameter minimization with respect \bar{p} . This approximation is well justified because the solar antineutrino probability is

clearly very small, We avoid in this way the simultaneous minimization with respect to the three parameters $(\bar{p}, \Delta m^2, \theta)$.

We perform a minimization of the one dimensional function $\chi^2(\bar{p})$. to test a particular oscillation hypothesis against the parameters of the best fit and obtain the allowed interval in \bar{p} parameter space taking into account the asymptotic properties of the likelihood function, i.e. $\log \mathcal{L} - \log \mathcal{L}_{min}$ behaves asymptotically as a χ^2 with one degree of freedom. In our case, the minimization can be performed analytically because of the simple, lineal, dependence. A given point in the confidence interval is allowed if the globally subtracted quantity fulfills the condition $\Delta\chi^2 = \chi^2(\bar{p}) - \chi_{min}^2 < \chi_n^2(CL)$. Where $\chi_{n=1}^2(90\%, 95\%, \dots) = 2.70, 3.84, \dots$ are the quantiles for one degree of freedom.

Restricting to physical values of \bar{p} , the minimum of the χ^2 function is obtained for $\bar{p} = 0$. The corresponding confidence intervals are $\bar{p} < 4.5\%$ (90% CL) and $\bar{p} < 7.0\%$ (95% CL). We have explicitly checked, varying the concrete place where the division between “Gaussian” and “poissonian” bins is established that the values of these upper limits are largely insensitive to details of our analysis. In particular, similar upper limits are obtained in the extreme cases: if Gaussian or poissonian statistics is employed for all 13 bins. These upper limits are considerably weaker than those obtained in the next section. One possible reason for that is that they are obtained applying asymptotic general arguments to the χ^2 distribution, stronger, or more precise limits could be obtained if a Monte Carlo simulation of the distribution of the finite sample χ^2 distribution is performed (where the boundary condition $\bar{p} > 0$ should be properly included).

Analysis of the global rate and highest energy bins

We can make an estimation of the upper bound on the appearance solar electron antineutrino probability simply counting the number of observed events and subtracting the number of events expected from the best-fit oscillation solution. For our purposes this difference, which in this case is positive, can be interpreted as a hypothetical signal coming from solar antineutrinos ($\Delta m_0^2 = 6.9 \times 10^5 \text{ eV}^2, \sin^2 \theta_0 = 1$):

$$S_{solar} = \bar{p} \times S_{solar}^0 = S_{obs} - S_{react}(\Delta m_0^2, \sin^2 \theta_0). \quad (9)$$

Putting [1] $S_{obs} = 54.3 \pm 7.5$ and $S_{react}(\Delta m_0^2, \sin^2 \theta_0) = 49 \pm 1.3$, we obtain $S_{obs} - S_{react} < 64.8$ (67.2) at 90 (95)% CL. From these numbers, the corresponding limits on solar electron antineutrino appearance probability are $\bar{p} < 0.45\%$, 0.52% at 90 or 95% CL. These limits are valid for the neutrino energy range $E_\nu \sim 2 - 8 \text{ MeV}$. In this case, due to the large range, the limits are better interpreted as limits on an energy-averaged probability according to expression 4.

In a similar approach, we use on continuation the binned KamLAND signal corresponding to the four highest energy bins (see Fig.3) which, as we will see, provide the strongest statistical significance and bounds. The reason for that is that the experiment KamLAND does not observe any signal here and, furthermore, the expected

signal from oscillating neutrinos with LMA parameters is negligibly small. Due to the small sample, we apply Poisson statistics to any of these bins and use the fact that a sum of Poisson variables of mean μ_i is itself a Poisson variable of mean $\sum \mu_i$. The background (here the reactor antineutrinos) and the signal (solar electron antineutrinos) are assumed to be independent Poisson Random variables with known means. If no events are observed, and, in particular, no background is observed, the unified intervals [37, 43] $[0, \epsilon_{CL}]$ are $[0, 2.44]$ at 90% CL and $[0, 3.09]$ at 95% CL. From here, we obtain $\bar{p} \times S_0^{solar} < \epsilon_{CL}$ or $\bar{p} < \epsilon_{CL}/S_0^{solar}$. Taking the expected number of events in the first 145 days of data taking and in this energy range (6-8 MeV) we obtain: $\bar{p} < 0.12\%$ (90% CL) and $\bar{p} < 0.15\%$ (95% CL).

5 A model for solar antineutrino production in the sun convection zone

The combined action of spin flavor precession in a magnetic field and ordinary neutrino matter oscillations can produce an observable flux of $\bar{\nu}_{eR}$'s from the Sun in the case of the neutrino being a Majorana particle. In the simplest model, where a thin layer of highly chaotic of magnetic field is assumed at the bottom of the convective zone (situated at $R \sim 0.7R_\odot$), the antineutrino appearance probability at the exit of the layer $P(\bar{\nu})$ is basically equal to the appearance probability of antineutrinos at the earth [19, 20] (see also Refs.[44] for some recent studies on RSFP solutions to the Solar Neutrino Problem). The quantity $P(\bar{\nu})$ is in general a function of the neutrino oscillation parameters $(\Delta m^2, \theta)$, the neutrino intrinsic magnetic moment and also of the neutrino energy and the characteristics and magnitude of the solar magnetic field. However, in a accurate enough approximation, such probability can be factorized in a term depending only on the oscillation parameters and another one depending only on the spin-flavor precession parameters:

$$P(\bar{\nu}) = \frac{1}{2}P_{e\mu}(\Delta m^2, \theta) \times [1 - \exp(-4\Omega^2\Delta r)] \quad (10)$$

where $P_{e\mu}$ is the $e-\mu$ solar conversion probability. We will assume in this work the LMA central values for $(\Delta m^2, \theta)$ obtained from recent KamLAND data and which are compatible with the SNO observations in solar neutrinos [45], we will take $P_{e\mu}(\Delta m^2, \theta) \simeq \langle P_{e\mu} \rangle^{exp, SNO} \simeq 0.4$. The second factor appearing in the expression contains the effect of the magnetic field. This quantity depends on the layer width Δr ($\sim 0.1R_\odot$) and $\Omega^2 \equiv \frac{1}{3}L_0\mu^2\langle B^2 \rangle$, where $\langle B^2 \rangle$ the r.m.s strength of the magnetic field and L_0 is a scale length ($L_0 \sim 1000$ km). For small values of the argument we have the following approximate expression which is accurate enough for many applications

$$P(\bar{\nu}) \simeq P_{e\mu} \times 2\Omega^2\Delta r = \kappa \mu^2\langle B^2 \rangle$$

the solar astrophysical factor $\kappa \equiv 2/3P_{e\mu}L_0\Delta r$ is numerically $\kappa^{LMA} \simeq 2.8 \times 10^{-44}$ MeV⁻². Upper limits on the antineutrino appearance probability can be translated into upper limits on the neutrino transition magnetic moment and the magnitude of the magnetic field in the solar interior. The results of the Formula 10 can be seen in Figure 3. An upper bound $\bar{p} < 0.15 - 0.20\%$ (95% CL) implies an upper limit on the product of the intrinsic neutrino magnetic moment and the value of the convective solar magnetic field as $\mu B < 2.3 \times 10^{-21}$ MeV (95% CL). In Fig.3 we show the antineutrino probability as a function of the magnetic moment μ for fixed values of the magnitude of the magnetic field. For realistic values of other astrophysical solar parameters ($L_0 \sim 1000$ km, $\Delta r \sim 0.1 R_\odot$), these upper limits would imply that the neutrino magnetic moment is constrained to be, in the most desfavoured case,

$\mu \leq 3.9 \times 10^{-12} \mu_B$ (95% CL) for a relatively small field $B = 50$ kG. Stronger limits are obtained for slightly higher values of the magnetic field: $\mu \leq 9.0 \times 10^{-13} \mu_B$ (95% CL) for field $B = 200$ kG and $\mu \leq 2.0 \times 10^{-13} \mu_B$ (95% CL) for field $B = 1000$ kG. Let us note that these assumed values for the magnetic field at the base the solar convective zone are relatively mild and well within present astrophysical expectatives.

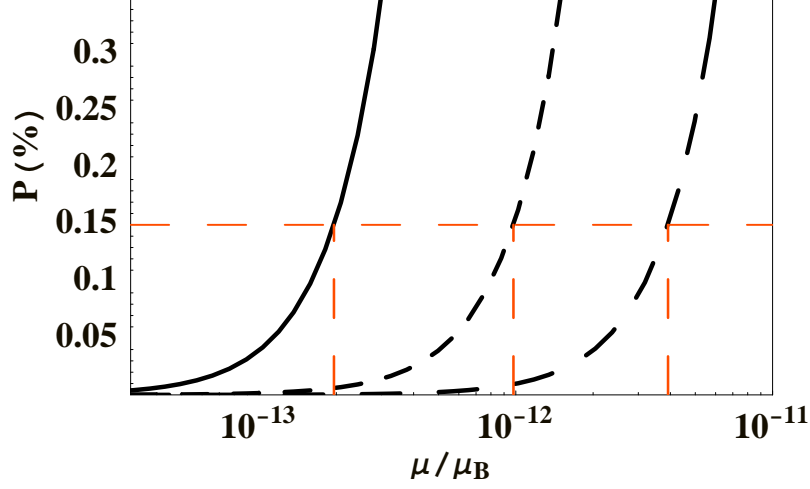


Figure 3: The solar antineutrino appearance probability \bar{p} as a function of the transition neutrino magnetic moment, in units of Bohr magnetons μ_B , for fixed values of the r.m.s solar magnetic field (Formula 10). From left (solid) to right (dashed), curves correspond to $B = 1000, 200, 50$ kG. From the curves, an upper limit $\bar{p} < 0.15\%$ implies $\mu < 1.9 \times 10^{-13} \mu_B, 9.0 \times 10^{-13} \mu_B, 3.0 \times 10^{-12} \mu_B$ respectively for each of the magnetic field above.

6 The magnetic field in the sun core

6.1 The solar antineutrino probability in core conversions

We start (see Ref.[16]) with the probability that a ν_{eL} produced inside the sun will reach the earth as a $\bar{\nu}_{eR}$

$$P(\nu_{eL} \rightarrow \bar{\nu}_{eR}) = P(\nu_{eL} \rightarrow \bar{\nu}_{\mu R}; R_S) \times P(\bar{\nu}_{\mu R} \rightarrow \bar{\nu}_{eR}; R_{es}) \quad (11)$$

in which the first term is the SFP probability, R_S is the solar radius and the second term is given by the well known formula for vacuum oscillations

$$P(\bar{\nu}_{\mu R} \rightarrow \bar{\nu}_{eR}; R_{es}) = \sin^2 2\theta \sin^2 \left(\frac{\Delta m^2}{4E} R_{es} \right) = \frac{1}{2}. \quad (12)$$

Here R_{es} is the distance between the sun and the earth and the rest of the notation is standard. Since $1.8 \text{ MeV} < E < 15 \text{ MeV}$ and, for LMA, $\Delta m^2 = 6.9 \times 10^{-5} \text{ eV}^2$, $\sin^2 2\theta = 1$ [27], we take the $\bar{\nu}_{\mu R} \rightarrow \bar{\nu}_{eR}$ vacuum oscillations to be in the averaging regime.

The SFP amplitude in perturbation theory for small μB is [7]¹

$$A(\nu_{eL} \rightarrow \bar{\nu}_{\mu R}) = \frac{\mu B(r_i) \sin^2 \theta(r_i)}{g_2'(r_i)}. \quad (13)$$

A key observation is that the antineutrino appearance probability is dependent on the production point of its parent neutrino so that the overall antineutrino probability is

$$P(\nu_{eL} \rightarrow \bar{\nu}_{eR}) = \frac{1}{2} \int |A(\nu_{eL} \rightarrow \bar{\nu}_{\mu R})|^2 f_B(r_i) dr_i \quad (14)$$

where f_B represents the neutrino production distribution function for Boron neutrinos [25] and the integral extends over the whole production region. As shall be seen, owing to this integration, the energy shape of probability (6) is largely insensitive to the magnetic field profile.

As mentioned above, for the LMA solution only the solar field profile in the neutrino production region [7] can affect the antineutrino flux. Hence we will discuss three profiles which span a whole spectrum of possibilities at this region. We study from a vanishing field (profile 1) to a maximum field at the solar center, with, in this second case, either a fast decreasing field intensity (profile 2) or a nearly flat one (profile 3) in the solar core (see fig. 4, lower panel). Thus, we consider respectively the following three profiles

Profile 1

$$B(r) = B_0 [\cosh(9r) - 1] \quad , \quad |r| \leq r_c \quad (15)$$

¹For notation we refer the reader to ref. [7].

$$B(r) = B_0 / \cosh[25(r - r_R)] \quad , \quad |r| > r_c, \quad (16)$$

with $r_c = 0.08$, $r_R = 0.16$,

Profile 2

$$B(r) = B_0 / \cosh(15r) \quad , \quad |r| \geq 0, \quad (17)$$

Profile 3

$$B(r) = B_0 [1 - (r/r_c)^2] \quad , \quad |r| \leq r_c, \quad (18)$$

with $r_c = 0.713$.

We also show in fig. 4 (upper panel) the 8B production distribution spectrum, so that a comparison between the strength of the field and the production intensity can be directly made.

The antineutrino production probabilities as a function of energy for each of these profiles are given in fig. 4. In the first panel, the values of the peak field are chosen so as to produce a fixed number of events. In this case the probability curves differ only slightly in their shapes while their normalizations are the same. The curves are in any case similar to the SFP survival probability ones [30] in the same energy range. In the second panel of fig. 4 the antineutrino probabilities for a common value of the peak field and these three different profiles are shown. It is hence apparent from these two graphs how the distribution of the magnetic field intensity is determinant for the magnitude of the antineutrino probability, but not for its shape. One important reason for this behavior is that we have integrated the antineutrino probability over the Boron production region.

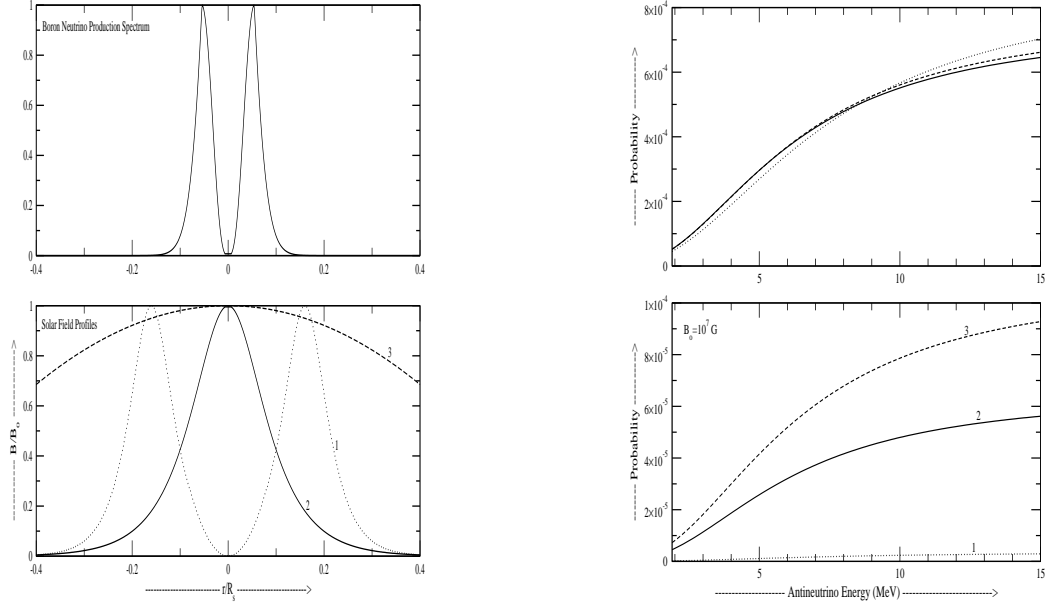


Figure 4: (LEFT) Upper panel: ^8B neutrino production spectrum (in arbitrary units) as a function of the radial coordinate. Lower panel: the three solar field profiles considered in the main text normalized to B_0 , the peak field value. (RIGHT) Antineutrino probabilities for solar field profiles 1, 2 and 3. Upper panel: the peak field is chosen in each case so as to produce the same event rate in KamLAND, (see the main text). Lower panel: the same value of the peak field ($B_0 = 10^7 \text{ G}$) is seen in each case to lead to probabilities of quite different magnitudes.

7 Results for the Magnetic Profile

The antineutrino signal for any magnetic field profile $B(r)$ can be written, taking into account the previous formulas and the near invariance of the probability shape (see fig. 4), as

$$S_{\bar{\nu}}[B(r)] = \alpha S_{\bar{\nu}}^0 \quad (19)$$

where $S_{\bar{\nu}}^0$ is the antineutrino signal taken at some nominal reference value B_0^0 for the field at the solar core for a certain reference profile B^0 . This profile dependent parameter α , being a ratio of two event rates given by eq.(7) for different profiles, can thus be simplified to

$$\alpha = \frac{\int \left(\frac{B(r_i) \sin^2 \theta(r_i)}{g_2(r_i)} \right)^2 f_B(r_i) dr_i}{\int \left(\frac{B^0(r_i) \sin^2 \theta(r_i)}{g_2(r_i)} \right)^2 f_B(r_i) dr_i} \quad (20)$$

where the integrals extend over the production region. As we mentioned before, for concreteness we have fixed along this discussion the neutrino magnetic moment $\mu_\nu = 10^{-12} \mu_B$.

We will now obtain bounds on parameter α and the peak field B_0 for each profile derived from KamLAND data, applying Gaussian probabilistic considerations to the global rate in the whole energy range, $E_\nu = (2.6-8.125) \text{ MeV}$, and Poissonian considerations to the event content in the highest energy bins ($E_e > 6 \text{ MeV}$) where KamLAND observes zero events. We denote by $S_{\bar{\nu}}^0$ the event rate with $B_0 = 10^7 G$ for each given profile ($S_{\bar{\nu}}^0 = S_{\bar{\nu}}(10^7 G)$). Taking the number of observed events and subtracting the number of events expected from the best-fit oscillation solution $[(\Delta m^2, \sin^2 2\theta)_{LMA} = (6.9 \times 10^{-5} \text{ eV}^2, 1)]$ and interpreting this difference as a hypothetical signal coming from solar antineutrinos, we have

$$S_{\bar{\nu}}^{sun} = S_{obs} - S_{react}(LMA). \quad (21)$$

Inserting [39] $S_{obs} = 54.3 \pm 7.5$ and $S_{react}(LMA) = 49 \pm 1.3$, we obtain $S_{obs} - S_{react} = \alpha S_{\bar{\nu}}^0 < 17.8 \text{ (20.2)}$ at 90 (95)% CL. Within each specific profile it is seen from (20) that the quantity α is simplified to $\alpha = (B_0/10^7 G)^2$, so that the previous inequality becomes

$$B_0^2 < \frac{S_{\bar{\nu}}^{sun}}{S_{\bar{\nu}}^0} (10^7 G)^2. \quad (22)$$

In this way we can derive for each given profile an upper bound on B_0 . The quantity $S_{\bar{\nu}}^0$ for profiles 1, 2 and 3 and the respective upper bounds on B_0 are shown in table 1. These upper limits can be cast in a more general way if do not fix the neutrino magnetic moment. To this end we will consider an arbitrary reference value $\mu_\nu^0 = 10^{-12} \mu_B$. Then within each profile, $\alpha = (\mu_\nu B_0 / \mu_\nu^0 10^7 G)^2$, where in the numerator and denominator we have respectively the peak field value and some reference peak field value of the

same profile. In the same manner as before we can derive the upper bounds on $\mu_\nu B_0$ which are also shown in table 1.

From the definition of α (20) it follows that the upper bounds on the antineutrino flux are independent of the field profile. These turn out to be $\phi_{\bar{\nu}} < 0.0034\phi(^8B)$ and $\phi_{\bar{\nu}} < 0.0038\phi(^8B)$ for 90 and 95% CL respectively.

We can similarly and independently apply Poisson statistics to the five highest energy bins of the KamLAND experiment. No events are observed in this region and the expected signal from oscillating neutrinos with LMA parameters is negligibly small. We use the fact that the sum of Poisson variables of mean μ_i is itself a Poisson variable of mean $\sum \mu_i$. The background (here the reactor antineutrinos) and the signal (the solar antineutrinos) are assumed to be independent Poisson random variables with known means. If no events are observed and in particular no background is observed, the unified intervals [31, 43] $[0, \epsilon_{CL}]$ are $[0, 2.44]$ at 90% CL and $[0, 3.09]$ at 95% CL.

From here, we obtain $\alpha S_{\bar{\nu}}^0 < \epsilon_{CL}$ or $\alpha < \epsilon_{CL}/S_{\bar{\nu}}^0$. Hence, as in the previous case, we have

$$B_0^2 < \frac{\epsilon_{CL}}{S_{\bar{\nu}}^0} (10^7 G)^2. \quad (23)$$

Using the expected number of events in the first 145 days of data taking and in this energy range $(6 - 8.125) \text{ MeV}$, we have derived upper bounds on B_0 (90 and 95% CL) for all three profiles. They are shown in table 2 along with the upper bounds on $\mu_\nu B_0$ taking μ_ν as a free parameter. The antineutrino flux upper bounds are now $\phi_{\bar{\nu}} < 0.0049\phi(^8B)$ $\phi_{\bar{\nu}} < 0.0055\phi(^8B)$ at 90 and 95% CL respectively. The KamLAND expected signal for an arbitrary field profile corresponding to 95% CL is shown in fig. 3.

The differences in magnitude among the bounds on B_0 and $\mu_\nu B_0$ presented in tables 1 and 2 for the different profiles are easy to understand. In fact, recalling that the 8B production zone peaks at 5% of the solar radius and becomes negligible at approximately 15% (fig. 4), then in order to generate a sizeable antineutrino flux, the magnetic field intensity should lie relatively close to its maximum in the range where the neutrino production is peaked. Thus for profile 1 the value of B_0 required to produce the same signal is considerably larger than for the other two, while profile 3 is the most efficient one for antineutrino production.

As referred to above, for different field profiles the probability curves will differ only slightly in their shape if they lead to the same number of events. In other words, for a given number of events the probability curves are essentially the same, regardless of the field profile, a fact illustrated in fig. 4. As a consequence, the energy spectrum of the expected solar antineutrino flux will be nearly the same for any profile. In fig. 6 we plot this profile independent spectrum together with the 8B one [25], so that a comparison can be made showing the shift in the peak and the distortion introduced.

Profile	$S_\nu^0(10^7 G)$	$B_0(90\%CL)$ G	$B_0(95\%CL)$ G	$\mu_\nu B_0(90\%CL)$ MeV	$\mu_\nu B_0(95\%CL)$ MeV
1.	0.006	5.27×10^8	5.62×10^8	3.05×10^{-18}	3.25×10^{-18}
2.	0.137	1.14×10^8	1.21×10^8	6.60×10^{-19}	7.04×10^{-19}
3.	0.224	8.92×10^7	9.50×10^7	5.16×10^{-19}	5.50×10^{-19}

Table 2: Solar antineutrino event rates, upper bounds on the peak field value for $\mu_\nu = 10^{-12}\mu_B$ and on $\mu_\nu B_0$ for arbitrary μ_ν and B_0 , assuming Gaussian statistics in the whole KamLAND spectrum.

Profile	$S_\nu^0(10^7 G)$	$B_0(90\%CL)$ G	$B_0(95\%CL)$ G	$\mu_\nu B_0(90\%CL)$ MeV	$\mu_\nu B_0(95\%CL)$ MeV
1.	0.004	2.53×10^8	2.85×10^8	1.47×10^{-18}	1.65×10^{-18}
2.	0.079	5.56×10^7	6.25×10^7	3.22×10^{-19}	3.62×10^{-19}
3.	0.130	4.34×10^7	4.88×10^7	2.51×10^{-19}	2.82×10^{-19}

Table 3: Same as table 1 assuming Poissonian statistics in the KamLAND energy range $E_e = (6 - 8.125) MeV$.

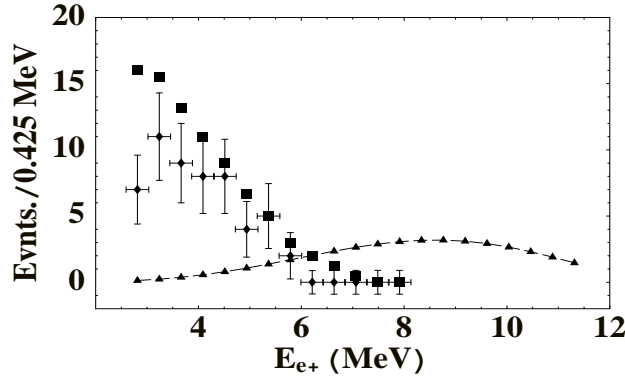


Figure 5: The solid squares represent the MC expectation of the KamLAND positron spectrum from reactor antineutrinos with no oscillations and the points with error bars represent the measured spectrum (from Fig.5 in Ref.[27]). Solid triangles represent the positron spectrum from solar antineutrinos (multiplied by 5) assuming profile 3 with peak field given by its 95% CL upper limit ($B_0 = 4.88 \times 10^7 G$). All curves refer to the same time exposure of 145 days.

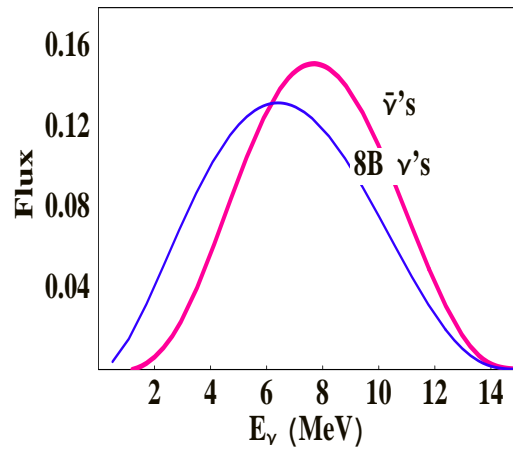


Figure 6: The expected solar antineutrino spectrum and the 8B neutrino one [25], both normalized to unity, showing the peak shift and the distortion introduced by the antineutrino probability.

8 Conclusions

In summary in this work we investigate the possibility of detecting solar antineutrinos with the KamLAND experiment. These antineutrinos are predicted by spin-flavor solutions to the solar neutrino problem.

The KamLAND experiment is sensitive to potential antineutrinos originated from solar ${}^8\text{B}$ neutrinos. We find that the results of the KamLAND experiment put relatively strict limits on the flux of solar electron antineutrinos $\Phi({}^8B) < 1.1 - 3.5 \times 10^4 \text{ cm}^{-2} \text{ s}^{-1}$, and their energy averaged appearance probability ($P < 0.15 - 0.50\%$). These limits are largely independent from any model on the solar magnetic field or any other astrophysical properties. As we remarked in Section 2.1, these upper limits on antineutrino probabilities and fluxes are still valid even if the antineutrino probabilities are significantly different from constant.

Next we assume a concrete model for antineutrino production where they are produced by spin-flavor precession in the convective solar magnetic field. In this model, the antineutrino appearance probability is given by a simple expression as $P(\bar{\nu}) = \kappa \mu^2 \langle B^2 \rangle$ with $\kappa^{LMA} \simeq 2.8 \times 10^{-44} \text{ MeV}^{-2}$. In the context of this model and assuming LMA central values for neutrino oscillation parameters ($\Delta m^2 = 6.9 \times 10^{-5} \text{ eV}^2$, $\sin^2 \theta = 1$) [1], the upper bound $\bar{p} < 0.15\%$ (95% CL) implies an upper limit on the product of the intrinsic neutrino magnetic moment and the value of the convective solar magnetic field as $\mu B < 2.3 \times 10^{-21} \text{ MeV}$ (95% CL). For realistic values of other astrophysical solar parameters these upper limits would imply that the neutrino magnetic moment is constrained to be, in the most desfavoured case, $\mu \leq 3.9 \times 10^{-12} \mu_B$ (95% CL) for a relatively small field $B = 50 \text{ kG}$. For slightly higher values of the magnetic field: $\mu \leq 9.0 \times 10^{-13} \mu_B$ (95% CL) for field $B = 200 \text{ kG}$ and $\mu \leq 2.0 \times 10^{-13} \mu_B$ (95% CL) for field $B = 1000 \text{ kG}$. These assumed values for the magnetic field at the base the solar convective zone are relatively mild and well within present astrophysical expectatives.

To conclude, now that SFP is ruled out as a dominant effect for the solar neutrino deficit, it is important to investigate its still remaining possible signature in the solar neutrino signal, namely an observable $\bar{\nu}_e$ flux. Our main conclusion is that, from the antineutrino production model expound here, an upper bound on the solar antineutrino flux can be derived, namely $\phi_{\bar{\nu}} < 3.8 \times 10^{-3} \phi({}^8B)$ and $\phi_{\bar{\nu}} < 5.5 \times 10^{-3} \phi({}^8B)$ at 95% CL, assuming respectively Gaussian or Poissonian statistics. For 90% CL we found $\phi_{\bar{\nu}} < 3.4 \times 10^{-3} \phi({}^8B)$ and $\phi_{\bar{\nu}} < 4.9 \times 10^{-3} \phi({}^8B)$ which shows an improvement relative to previously existing bounds from LSD [32] by a factor of 3-5. These are independent of the detailed magnetic field profile in the core and radiative zone and the energy spectrum of this flux is also found to be profile independent. We also derive upper bounds on the peak field value which are uniquely determined for a fixed solar field profile. In the most efficient antineutrino producing case (profile 3), we get (95% CL) an upper limit on the product of the neutrino magnetic moment by the solar field

$\mu_\nu B \leq 2.8 \times 10^{-19}$ MeV or $B_0 \leq 4.9 \times 10^7 G$ for $\mu_\nu = 10^{-12} \mu_B$. A recent study of the magnetic field in the radiative zone of the sun has provided upper bounds of (3-7) MG [46] in that region in the vicinity of $0.2 R_S$ which are independent of any neutrino magnetic moment. Therefore we can use them in conjunction with our results to obtain a limit on μ_ν . Using $B_0 \sim 3 - 7 MG$, we get from the results for profiles 1-3: $\mu \leq 0.7 - 9.6 \times 10^{-12} \mu_B$. Moreover, from the limits obtained in this work, if the 'true' solar profile resembles either a profile like 1 or 3, this criterion implies that SFP cannot be experimentally traced in the next few years, since the peak field value must be substantially reduced in order to comply with this upper bound, thus leading to a much too small antineutrino probability to provide an observable event rate. On the other hand, for a profile like 2 or in general any one resembling a dipole field, SFP could possibly be visible.

References

- [1] K. Eguchi et al. [Kamland Collaboration], arXiv:hep-ex/0212021.
- [2] J. N. Bahcall, M. C. Gonzalez-Garcia and C. Pena-Garay, arXiv:hep-ph/0212147. A. Bandyopadhyay, S. Choubey, R. Gandhi, S. Goswami and D. P. Roy, arXiv:hep-ph/0212146. W. l. Guo and Z. z. Xing, arXiv:hep-ph/0212142. G. Barenboim, L. Borissov and J. Lykken, arXiv:hep-ph/0212116.
- [3] J. Schechter, J. W. F. Valle, Phys. Rev. D **24** (1981) 1883. J. Schechter, J. W. F. Valle, Phys. Rev. D **25** (1981) 283, Erratum.
- [4] C. S. Lim, W. J. Marciano, Phys. Rev. D **37** (1988) 1368.
- [5] E. Kh. Akhmedov, Sov. J. Nucl. Phys. 48 (1988) 382, Yad. Fiz. 48 (1988) 599 (in Russian). E. Kh. Akhmedov, Phys. Lett. B **213** (1988) 64.
- [6] E. Kh. Akhmedov, Sov. J. JETP 68 (1989) 690, Zh. Eksp. Teor. Fiz. 95 (1989) 1195 (in Russian). R. S. Raghavan, et al., Phys. Rev. D **44** (1991) 3786. C. S. Lim et al., Phys. Lett B **243** (1990) 389. E. Kh. Akhmedov, S. T. Petcov, A. Yu. Smirnov, Phys. Rev. D **48** (1993) 2167, hep-ph/9301211.
- [7] E. K. Akhmedov and J. Pulido, Phys. Lett. B **553**, 7 (2003) [arXiv:hep-ph/0209192].
- [8] M. Apollonio et al. (CHOOZ coll.), hep-ex/9907037, Phys. Lett. B **466** (1999) 415. M. Apollonio *et al.*, Phys. Lett. B **420** (1998) 397.
F. Boehm *et al.*, Phys. Rev. D **62** (2000) 072002 [hep-ex/0003022].
- [9] Y. F. Wang [Palo Verde Collaboration], Int. J. Mod. Phys. A **16S1B**, 739 (2001); F. Boehm *et al.*, Phys. Rev. D **64**, 112001 (2001).
- [10] P. Vogel and J. F. Beacom, Phys. Rev. D **60**, 053003 (1999) [arXiv:hep-ph/9903554].

- [11] G. Zacek et al. Phys. Rev. D **34**, 9 (1986) 2621.
- [12] F. Reines, R. M. Woods, Phys. Rev. Lett. **14** (1965) 20.
- [13] D. H. Wilkinson, Nucl. Phys. A **377**, 474 (1982).
- [14] L. De Braekeleer [KamLAND Collaboration], Nucl. Phys. Proc. Suppl. **87** (2000) 312.
J. Shirai, “Kamioka Liquid Scintillator Anti-Neutrino Detector”, Neutrino2002, May 25-30, Munich, Germany. A. Suzuki [KamLAND Collaboration], Nucl. Phys. Proc. Suppl. **77** (1999) 171.
- [15] E. Torrente-Lujan, JHEP **0304** (2003) 054 [arXiv:hep-ph/0302082].
- [16] B. C. Chauhan, J. Pulido and E. Torrente-Lujan, Phys. Rev. D **68** (2003) 033015 [arXiv:hep-ph/0304297]. B. C. Chauhan, J. Pulido and E. Torrente-Lujan, arXiv:hep-ph/0309068.
- [17] J. Shirai, “Start of Kamland”, talk given at *Neutrino 2002*, XXth International Conference on Neutrino Physics and Astrophysics, May 2002, Munich. Transparencies can be obtained from <http://neutrino2002.ph.tum.de>. See also: P. Alivisatos *et al.*, STANFORD-HEP-98-03.
- [18] P. Aliani, V. Antonelli, M. Picariello and E. Torrente-Lujan, JHEP **0302**:025, 2003.
- [19] E. Torrente-Lujan, *Prepared for 2nd ICRA Network Workshop: The Chaotic Universe: Theory, Observations, Computer Experiments, Rome, Italy, 1-5 Feb 1999*. E. Torrente-Lujan, arXiv:hep-ph/9912225. E. Torrente-Lujan, Phys. Rev. D **59**, 093006 (1999). E. Torrente-Lujan, Phys. Rev. D **59**, 073001 (1999). E. Torrente-Lujan, arXiv:hep-ph/9602398. V. B. Semikoz and E. Torrente-Lujan, Nucl. Phys. B **556**, 353 (1999). E. Torrente-Lujan, arXiv:hep-ph/0210037. E. Torrente Lujan, Phys. Rev. D **53**, 4030 (1996).
- [20] E. Torrente-Lujan, Phys. Lett. B **441**, 305 (1998).
- [21] J. N. Bahcall, M. H. Pinsonneault and S. Basu, Astrophys. J. **555**, 990 (2001).
- [22] Q. R. Ahmad *et al.* [SNO Collaboration], Phys. Rev. Lett. **89**, 011301 (2002).
- [23] Q. R. Ahmad *et al.* [SNO Collaboration], Phys. Rev. Lett. **89**, 011302 (2002).
- [24] P. Aliani, V. Antonelli, M. Picariello and E. Torrente-Lujan, New J. Phys. **5** (2003) 2 [arXiv:hep-ph/0207348]. P. Aliani, V. Antonelli, R. Ferrari, M. Picariello and E. Torrente-Lujan, arXiv:hep-ph/0205061.
- [25] J.N.Bahcall’s homepage, <http://www.sns.ias.edu/~jnb/>.
- [26] J. Busenitz et al. (US KamLand Coll). proposal for US Participation in KamLand. March 1999 (Unpublished).

- [27] K. Eguchi *et al.* [KamLAND Collaboration], Phys. Rev. Lett. **90**, 021802 (2003) [arXiv:hep-ex/0212021].
- [28] P. Aliani, V. Antonelli, R. Ferrari, M. Picariello and E. Torrente-Lujan, Phys. Rev. D **67** (2003) 013006.
- [29] A. Strumia, C. Cattadori, N. Ferrari and F. Vissani, arXiv:hep-ph/0205261. A. Bandyopadhyay, S. Choubey, S. Goswami and D. P. Roy, Phys. Lett. B **540**, 14 (2002). R. Foot and R. R. Volkas, arXiv:hep-ph/0204265.
- [30] J. Pulido and E. K. Akhmedov, Astropart. Phys. **13**, 227 (2000) [arXiv:hep-ph/9907399].
- [31] K. Hagiwara *et al.* [Particle Data Group Collaboration], Phys. Rev. D **66**, 010001 (2002).
- [32] M. Aglietta *et al.*, JETP Lett. **63** (1996) 791, Pisma Zh. Eksp. Teor. Fiz. **63** (1996) 753 (in Russian).
- [33] P. Aliani, V. Antonelli, R. Ferrari, M. Picariello and E. Torrente-Lujan, arXiv:hep-ph/0206308. S. Khalil and E. Torrente-Lujan, J. Egyptian Math. Soc. **9**, 91 (2001) [arXiv:hep-ph/0012203]. E. Torrente-Lujan, arXiv:hep-ph/9902339.
- [34] P. Aliani, V. Antonelli, M. Picariello and E. Torrente-Lujan, Nucl. Phys. **B634** (2002) 393-409. P. Aliani, V. Antonelli, M. Picariello and E. Torrente-Lujan, Nucl. Phys. Proc. Suppl. **110**, 361 (2002) [arXiv:hep-ph/0112101]. P. Aliani, V. Antonelli, R. Ferrari, M. Picariello and E. Torrente-Lujan, arXiv:hep-ph/0205061. P. Aliani, V. Antonelli, M. Picariello and E. Torrente-Lujan, arXiv:hep-ph/0309156.
- [35] V. Barger, D. Marfatia and K. Whisnant, arXiv:hep-ph/0106207.
- [36] E. Torrente-Lujan, Nucl. Phys. Proc. Suppl. **87**, 504 (2000). E. Torrente-Lujan, Phys. Lett. B **494**, 255 (2000).
- [37] “Review of Particle Properties”, K. Hagiwara *et al.* (Particle Data Group), Phys. Rev. D **66** (2002) 010001
- [38] P. Aliani, V. Antonelli, M. Picariello and E. Torrente-Lujan, New J. Phys. **5** (2003) 2. P. Aliani, V. Antonelli, R. Ferrari, M. Picariello and E. Torrente-Lujan, arXiv:hep-ph/0211062. P. Aliani, V. Antonelli, M. Picariello and E. Torrente-Lujan, JHEP **0302** (2003) 025 [arXiv:hep-ph/0208089].
- [39] G. Horton-Smith, *Neutrinos and Implications for Physics Beyond the Standard Model*, Stony Brook, Oct. 11-13, 2002. <http://insti.physics.sunysb.edu/itp/conf/neutrino.html> A. Suzuki. *Texas in Tuscany, XXI Symposium on Relativistic Astrophysics* Florence, Italy, December 9-13, 2002. <http://www.arcetri.astro.it/texaflor/>.
- [40] H. Murayama and A. Pierce, Phys. Rev. D **65** (2002) 013012.
- [41] P. Vogel, A. Engel, Phys. Rev. D **39**, 3378 (1989).

- [42] A. Piepke [Kamland collaboration], Nucl. Phys. Proc. Suppl. **91**, 99 (2001)
- [43] G. J. Feldman and R. D. Cousins, Phys. Rev. D **57**, 3873 (1998).
- [44] E. K. Akhmedov, arXiv:hep-ph/0207342. E. K. Akhmedov and J. Pulido, Phys. Lett. B **553**, 7 (2003). E. K. Akhmedov and J. Pulido, Phys. Lett. B **553**, 7 (2003). B. C. Chauhan, arXiv:hep-ph/0204160. B. C. Chauhan, S. Dev and U. C. Pandey, Phys. Rev. D **59**, 083002 (1999) [Erratum-ibid. D **60**, 109901 (1999)]. U. C. Pandey, B. C. Chauhan and S. Dev, Mod. Phys. Lett. A **13**, 3201 (1998). B. C. Chauhan and J. Pulido, Phys. Rev. D **66**, 053006 (2002). E. K. Akhmedov and J. Pulido, Phys. Lett. B **529**, 193 (2002). J. Pulido, Astropart. Phys. **18**, 173 (2002). E. K. Akhmedov and J. Pulido, Phys. Lett. B **485**, 178 (2000). J. Pulido and E. K. Akhmedov, Astropart. Phys. **13**, 227 (2000).
- [45] P. Aliani, V. Antonelli, M. Picariello and E. Torrente-Lujan, Phys. Rev. D **63**, 232345 (2003) [arXiv:hep-ph/0212212].
- [46] A. Friedland and A. Gruzinov, arXiv:astro-ph/0211377.